Dipole oscillations in Bose-Fermi mixtures in the time-dependent Gross-Pitaevskii and Vlasov equations

Tomoyuki Maruyama[1,2,3] and George F. Bertsch[1]
[1]*Institute for Nuclear Theory, University of Washington, Seattle, Washington 98195, USA*
[2]*College of Bioresource Sciences, Nihon University, Fujisawa 252-8510, Japan*
[3]*Advanced Science Research Center, Japan Atomic Energy Research Institute, Tokai 319-1195, Japan*
(Received 12 June 2007; revised manuscript received 9 April 2008; published 13 June 2008)

We study the dipole collective oscillations in Bose-Fermi mixtures in a dynamical time-dependent approach, which is formulated with the time-dependent Gross-Pitaevskii equation and the Vlasov equation. While the Bose gas oscillates monotonously, the fermion oscillation shows a beat and damping. We find big differences in behaviors of fermion oscillation between the time-dependent approach and usual approaches such as the sum-rule approach. When the amplitude is not minimal, the dipole oscillation of the Fermi gas cannot be described with a simple center-of-mass motion.

DOI: 10.1103/PhysRevA.77.063611 PACS number(s): 03.75.Kk, 67.30.H−, 51.10.+y

I. INTRODUCTION

Over the last several years, there have been significant progresses in the production of ultracold gases, which realize the Bose-Einstein condensates (BECs) [1–4], two boson mixtures [5], degenerate atomic Fermi gases [6], and Bose-Fermi (BF) mixing gases [7–9]. In particular the BF mixtures attract physical interest as a typical example in which particles obeying different statistics are intermingled. Using this system we have a very big opportunity to get new various knowledge about many-body systems because we can make a large variety of combinations of atomic species and control the atomic interactions using the Feshbach resonance [10]. Theoretical studies of the BF mixtures have been done for static properties [11–16], for the phase diagram and phase separation [17–20], for stability [21–23], and for collective excitations [24–31].

Above all phenomena the spectrum of the collective excitations is an important diagnostic signal for these systems. Such oscillations are common to a variety of many-particle systems and are often sensitive to the interaction and the structure of the ground state and the excited states. Theoretically collective motions are usually studied with the random phase approximation (RPA) [26,28] or its approximate methods such as the sum-rule [29] and the scaling [30,32,33] approaches. The first author (T.M.) and his collaborators [31] studied monopole oscillations of BF mixtures by calculating the time evolution of these oscillations with the time-dependent Gross-Pitaevskii (TDGP) equation and the Vlasov equation. This dynamical approach showed different behaviors of the oscillation from RPA [28], such as rapid damping at zero temperature.

The RPA can treat only states with one-particle and one-hole excitation and only describe minimal vibrations around ground states; for example, it is shown in Ref. [28]. that the radial variation is only about 0.05% in RPA, while the amplitudes of actual experiments can be as large as 10% [34]. For the single boson system the RPA [35] explained experimental results on frequencies of collective motions well [34]. In this system all bosons occupy one single particle state at zero temperature, and their collective motions are simple; damping does not appear at very low temperature in experiments [36] and in a theoretical work with the time-dependent density matrix theory [37].

On the other hand, fermions occupy many single particle states even at zero temperature. When the amplitude is about 10% of root-mean-square radius, the monopole states have as large excited energy as ten to one-hundred times of the one-particle and one-hole excitation energy. Their collective oscillations with a large amplitude are multiparticle and multihole states and include various mode with different frequencies. Indeed an oscillation of population difference in two-component Fermi gas has shown damping due to a multimode dephasing [38]. In the BF mixtures, especially, fermions occupy a larger region than condensed bosons, and have different potentials between inside and outside of the boson occupation region. Then their motions are not harmonic, and then the fermion oscillation makes damping [31]. In order to study the collective oscillation in BF mixtures, hence, we need to calculate time evolution of the system using a time-dependent dynamical approach.

Thus the BF mixing gases show new dynamical properties different from those in other finite many-body system such as nuclei. In order to have more information on the dynamical properties, we need to investigate other kinds of multipole motions. In this paper we study the dipole oscillations in Bose-Fermi mixtures as the next step by solving the time evolution of the condensed boson wave function and the fermion phase-space distribution function with the TDGP equations and the Vlasov equations, respectively.

In the next section we explain our transport model to calculate the time evolution of the system. In Sec. III we show the calculational results for the dipole oscillation in the BF mixture, and discuss their properties. Then we summarize our work in Sec. IV.

II. TIME EVOLUTION EQUATIONS

Here we briefly explain our approach. In this work we consider a dilute boson and one-component-fermion coexistent gases at zero temperature with the axial symmetry with respect to the z axis. We assume only zero-range interaction

between atoms, and there is no fermion-fermion interaction in the system. The Hamiltonian is written as

$$\tilde{H} = \int d^3q \Bigg[-\frac{\hbar^2}{2M_B}\tilde{\phi}^\dagger(\boldsymbol{q})\nabla_q^2\tilde{\phi}(\boldsymbol{q}) + \frac{1}{2}M_B\Omega_B^2(\boldsymbol{q}_T^2 + \kappa_L^2 q_L^2)\tilde{\phi}^\dagger(\boldsymbol{q})\tilde{\phi}(\boldsymbol{q}) + \frac{2\pi\hbar^2 a_{BB}}{M_B}\{\tilde{\phi}^\dagger(\boldsymbol{q})\tilde{\phi}(\boldsymbol{q})\}^2 - \frac{\hbar^2}{2M_f}\tilde{\psi}^\dagger(\boldsymbol{q})\nabla_q^2\tilde{\psi}(\boldsymbol{q}) + \frac{1}{2}M_f\Omega_F^2(\boldsymbol{q}_T^2 + \kappa_L^2 q_L^2)\tilde{\psi}^\dagger(\boldsymbol{q})\tilde{\psi}(\boldsymbol{q}) + \frac{2\pi\hbar^2 a_{BF}}{M_r}\tilde{\phi}^\dagger(\boldsymbol{q})\tilde{\phi}(\boldsymbol{q})\tilde{\psi}^\dagger(\boldsymbol{q})\tilde{\psi}(\boldsymbol{q}) \Bigg], \tag{1}$$

where $\tilde{\phi}$ and $\tilde{\psi}$ are boson and fermion fields, respectively, M_B and M_F are the boson and fermion masses, $M_r \equiv M_B M_F/(M_B+M_F)$ is the reduced boson-fermion mass, Ω_B and Ω_F are the transverse trapped frequencies of the boson and the fermion, a_{BB} and a_{BF} are the s-wave scattering lengths between two bosons and between boson and fermion, respectively. In addition the positional coordinate is described as $\boldsymbol{q} \equiv (\boldsymbol{q}_T, q_L)$, and κ_L is the ratio of the longitudinal trapped frequency to the transverse trapped frequency.

In this formulation we can change all variables to dimensionless ones without losing generality as follows. We normalized the spatial coordinate $\boldsymbol{q}$ to the dimensionless coordinates $\boldsymbol{r}$ as $\boldsymbol{r} \equiv (\boldsymbol{r}_T, z) \equiv \boldsymbol{q}/R_B$ with $R_B = (\hbar/M_B\Omega_B)^{1/2}$. According to this normalization the boson and fermion fields are also scaled as $\phi(\psi) = R_B^{-1/3}\tilde{\phi}(\tilde{\psi})$. By dividing the above Hamiltonian $\bar{H}$ by $\hbar\Omega_B$, we can define the dimensionless Hamiltonian $H \equiv \tilde{H}/\hbar\Omega_B$ as

$$H = \int d^3r \Bigg[-\frac{1}{2}\phi^\dagger(\boldsymbol{r})\nabla_r^2\phi(\boldsymbol{r}) + \frac{1}{2}(\boldsymbol{r}_T^2 + \kappa_L^2 z^2)\phi^\dagger(\boldsymbol{r})\phi(\boldsymbol{r}) + \frac{g_{BB}}{2}\{\phi^\dagger(\boldsymbol{r})\phi(\boldsymbol{r})\}^2 - \frac{1}{2m_f}\psi^\dagger(\boldsymbol{r})\nabla_r^2\psi(\boldsymbol{r}) + \frac{1}{2}m_f\omega_f^2(\boldsymbol{r}_T^2 + \kappa_L^2 z^2)\psi^\dagger(\boldsymbol{r})\psi(\boldsymbol{r}) + h_{BF}\phi^\dagger(\boldsymbol{r})\phi(\boldsymbol{r})\psi^\dagger(\boldsymbol{r})\psi(\boldsymbol{r}) \Bigg], \tag{2}$$

where $m_f \equiv M_F/M_B$, $\omega_f \equiv \Omega_F/\Omega_B$, and $g_{BB} \equiv 8\pi\hbar a_{BB}R_B^{-1}$ and $h_{BF} \equiv 4\pi\hbar m_f a_{BF}(1+m_f)^{-1}R_B^{-1}$.

In this work we consider the zero-temperature system, including N_b bosons and N_f fermions, so that the total wave function is written as

$$\Phi(\tau) = \left\{ \prod_{i=1}^{N_b} \phi_c(\boldsymbol{r}_i) \right\} \Psi_f[\psi_n], \tag{3}$$

where ϕ_c is a wave function of the condensed boson and Ψ_f is a Slater determinant of fermions with single particle wave functions, ψ_n. The time evolution of the wave functions are obtained from the variational condition that

$$\delta \int d\tau \langle\Phi(\tau)| \left\{ i\frac{\partial}{\partial\tau} - H \right\} |\Phi(\tau)\rangle = 0. \tag{4}$$

From this condition we derive coupled equations of the TDGP and time-dependent Hartree Fock (TDHF) equations as follows:

$$i\frac{\partial}{\partial\tau}\phi_c(\boldsymbol{r},\tau) = \left\{ -\frac{1}{2}\nabla_r^2 + U_B(\boldsymbol{r}) \right\} \phi_c(\boldsymbol{r},\tau), \tag{5}$$

$$i\frac{\partial}{\partial\tau}\psi_n(\boldsymbol{r},\tau) = \left\{ -\frac{1}{2m_f}\nabla_r^2 + U_F(\boldsymbol{r}) \right\} \psi_n(\boldsymbol{r},\tau) \tag{6}$$

with

$$U_B(\boldsymbol{r}) = \frac{1}{2}(\boldsymbol{r}_T^2 + \kappa_L^2 z^2) + g_{BB}\rho_B(\boldsymbol{r}) + h_{BF}\rho_F(\boldsymbol{r}), \tag{7}$$

$$U_F(\boldsymbol{r}) = \frac{1}{2}m_f\omega_f^2(\boldsymbol{r}_T^2 + \kappa_L^2 z^2) + h_{BF}\rho_B(\boldsymbol{r}), \tag{8}$$

where ρ_B and ρ_F are boson and fermion densities which are given by

$$\rho_B(\boldsymbol{r}) = N_b|\phi_c(\boldsymbol{r})|^2, \tag{9}$$

$$\rho_F(\boldsymbol{r}) = \sum_n^{\text{occ}} |\psi_n(\boldsymbol{r})|^2. \tag{10}$$

The number of fermion states are usually too large to solve the above TDHF equations directly so instead one uses the semi-classical approach. In the semiclassical limit ($\hbar \to 0$) the TDHF equation is equivalent to the following Vlasov equation [39]:

$$\frac{d}{d\tau}f(\boldsymbol{r},\boldsymbol{p};\tau) = \left\{ \frac{\partial}{\partial\tau} + \frac{\boldsymbol{p}}{m_f}\boldsymbol{\nabla}_r - [\boldsymbol{\nabla}_r U_F(\boldsymbol{r})][\boldsymbol{\nabla}_p] \right\} f(\boldsymbol{r},\boldsymbol{p};\tau) = 0, \tag{11}$$

where $f(\boldsymbol{r},\boldsymbol{p};\tau)$ is the fermion phase-space distribution function defined as

$$f(\boldsymbol{r},\boldsymbol{p},\tau) = \int d^3u \langle\Phi|\psi^\dagger\left(\boldsymbol{r} - \frac{1}{2}\boldsymbol{u},\tau\right)\psi\left(\boldsymbol{r} + \frac{1}{2}\boldsymbol{u},\tau\right)|\Phi\rangle e^{-i\boldsymbol{p}\boldsymbol{u}}. \tag{12}$$

As an actual numerical method we introduce the test particle method [40] to solve the Vlasov Eq. (11) and describe the fermion phase-space distribution function as

$$f(\boldsymbol{r},\boldsymbol{p},\tau) = \frac{(2\pi)^3}{\tilde{N}_T}\sum_{i=1}^{\tilde{N}_T N_f} \delta\{\boldsymbol{r} - \boldsymbol{r}_i(\tau)\}\delta\{\boldsymbol{p} - \boldsymbol{p}_i(\tau)\}, \tag{13}$$

where $\tilde{N}_T$ is the number of test-particles per fermion.

By substituting Eq. (13) into Eq. (11), we can obtain the following equations of motion for test-particles:

$$\frac{d}{d\tau}\boldsymbol{r}_i(\tau) = \frac{\boldsymbol{p}_i}{m_f}, \tag{14}$$

$$\frac{d}{d\tau}\boldsymbol{p}_i(\tau) = -\nabla_r U_F(\boldsymbol{r}). \tag{15}$$

Thus we obtain the time evolutions of the condensed boson wave function and the fermion phase space distribution function by solving Eqs. (5), (14), and (15).

III. RESULTS AND DISCUSSIONS

In this section we show the results of our calculations on the dipole oscillations in the BF mixture. We deal with the system ^{87}Rb-^{40}K, where the number of the bosons (^{87}Rb) and the fermions (^{40}K) are $N_b=10000$ and $N_f=1000$, respectively, and the fermion mass normalized by boson mass is $m_f=40/87\approx 0.46$. We assume the spherical trap ($\kappa_L=1$) and take the fermion trapped frequency to be $\omega_f=1/\sqrt{m_f}\approx 1.48$. The boson-boson interaction parameter g_{BB} is fixed to be $g_{BB}=1.34\times 10^{-2}$ [41], which corresponds to $a_{BB}=4.22$ nm, while the BF interaction parameter h_{BF} is varied. In the numerical calculation we take the number of the test-particles per fermion to be $\tilde{N}=100$ and solve the time evolutions by using the second order predictor-corrector method.

A. Ground state

The sum-rule approach [29] showed that the dipole oscillation frequency is sensitive to the density distributions. In this subsection, then, we see the boson and fermion density distribution from the point of view of the boson-fermion coupling dependence.

In the ground state the wave function of the condensed boson ϕ_c is defined as a solution of the following Gross-Pitaevskii equation:

$$\left\{-\frac{1}{2}\nabla_r^2 + \frac{1}{2}(\boldsymbol{r}_T^2 + \kappa_L^2 z^2) + g_{BB}\rho_B(\boldsymbol{r}) + h_{BF}\rho_F(\boldsymbol{r})\right\}\phi_c^{(g)}(\boldsymbol{r}) = \mu_b\phi_c^{(g)}(\boldsymbol{r}), \tag{16}$$

where μ_b is the boson chemical potential. In the ground state the fermion phase-space distribution function is given by the Thomas-Fermi (TF) approximation

$$f(\boldsymbol{r},\boldsymbol{p}) = \theta[\mu_f - \varepsilon(\boldsymbol{r},\boldsymbol{p})], \tag{17}$$

with

$$\varepsilon(\boldsymbol{r},\boldsymbol{p}) = \frac{1}{2m_f}\boldsymbol{p}^2 + U_F(\boldsymbol{r}), \tag{18}$$

where μ_f is the fermion chemical potential. In this TF approximation the fermion density ρ_F is obtained as the solution of the following equation:

$$\frac{1}{2m_f}\{6\pi^2\rho_F(\boldsymbol{r})\}^{2/3} + \frac{1}{2}m_f\omega_f^2(\boldsymbol{r}_T^2 + \kappa_L^2 z^2) + h_{BF}\rho_B(\boldsymbol{r}) = \mu_f. \tag{19}$$

Here we iterate solving the boson wave function with Eq. (16) and searching the Fermi energy μ_f in Eq. (19) to give the correct fermion number.

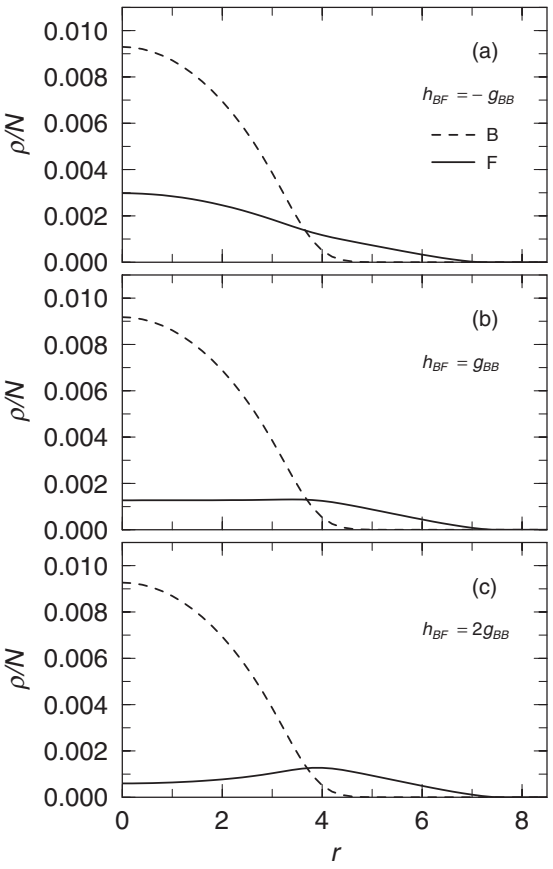

FIG. 1. The density distribution of the BF mixing gas with the boson-fermion coupling $h_{BF}=-g_{BB}$ (a), $h_{BF}=g_{BB}$ (b), and $h_{BF}=g_{BB}$ (c). The dashed and solid lines represent the density of the boson and Fermi gases, respectively.

In Fig. 1 we show the density distribution of the boson and Fermi gases with the boson-fermion coupling $h_{BF}=-g_{BB}$ (a), $h_{BF}=g_{BB}$ (b), and $h_{BF}=2g_{BB}$ (c). The solid and dashed lines represent the results of boson and Fermi gases, respectively. The density distribution of the Bose gas is negligibly changed while the fermion density distribution in the boson occupation region varies as the boson-fermion coupling increases. The fermion density distribution is central peaked when $h_{BF}=-g_{BB}$, flat when $h_{BF}=g_{BB}$, and surface peaked when $h_{BF}=2g_{BB}$.

This boson-fermion coupling dependence of the fermion density distribution can be easily explained as follows. When the boson number N_b is very large, the boson density distribution can also be given by the TF approximation as

$$\rho_B(\boldsymbol{r}) = \frac{1}{g_{BB}}\left[\mu_B - \frac{1}{2}(\boldsymbol{r}_T^2 + \kappa_L^2 z^2) - h_{BF}\rho_F(\boldsymbol{r})\right]. \tag{20}$$

Note that the boson density in Eq. (20) is defined within a region, and it is zero outside of that region.

Substituting Eq. (20) into Eq. (19), we can get

$$\frac{1}{2m_f}(6\pi^2\rho_F)^{2/3} - \frac{h_{BF}^2}{g_{BB}}\rho_F = \mu_F - \frac{h_{BF}}{g_{BB}}\mu_B - \frac{1}{2}\left(m_f\omega_f^2 - \frac{h_{BF}}{g_{BB}}\right)\xi^2, \tag{21}$$

where $\xi^2 \equiv r_T^2 + \kappa_L^2 z^2$. From this equation we can easily know that ρ_F=const when $h_{BF}/g_{BB}=1$ and $\rho_B>0$. Furthermore the derivative of the fermion density ρ_F with respect to ξ is given by

$$\left(\frac{4\pi^4}{3m_f^3}\right)^{1/3}\left\{\rho_F^{-1/3} - \frac{3m_f^3h_{BF}^6}{4\pi^4 g_{BB}^3}\right\}\frac{1}{\xi}\frac{\partial\rho_F}{\partial\xi} = -\left(m_f\omega_f^2 - \frac{h_{BF}}{g_{BB}}\right). \tag{22}$$

The stability condition [18], that $(\partial\mu_b/\partial\rho_B)(\partial\mu_f/\partial\rho_F) - (\partial\mu_b/\partial\rho_F)(\partial\mu_f/\partial\rho_B) > 0$, restricts the value of the fermion density as $\rho_F < 4\pi^4 g_{BB}^3/3m_f^3h_{BF}^6$. In the boson occupation region, therefore, the derivative of the fermion density is negative $\partial\rho_F/\partial\xi<0$ when $h_{BF}/g_{BB} > m_f\omega_f^2$ and positive $\partial\rho_F/\partial\xi > 0$ when $h_{BF}/g_{BB} > m_f\omega_f^2$.

As mentioned before, we take the parameters to be $m_f\omega_f^2=1$ and $\kappa_L=1$ in the present calculation. Thus the TF approximation can explain the relation between the boson-fermion coupling and the fermion density distributions.

B. Dipole oscillation

In this subsection we show our actual results of the numerical simulations on the dipole oscillations. Here we define the center of mass (c.m.) position on z coordinates for bosons and fermions as z_B and z_F, respectively. We will discuss the oscillation behavior by examining the time dependence of z_B and z_F.

In actual simulations we boost the condensed boson wave function and the fermion test-particles at the starting time $\tau=0$ in the following way:

$$\phi_c(\boldsymbol{r}, \tau=0) = e^{i\lambda_B z}\phi_c^{(g)}(\boldsymbol{r}), \tag{23}$$

$$p_z(i) = p_z^{(g)}(i) + m_f\omega_f\lambda_F \tag{24}$$

with the boost parameters λ_B and λ_F, where the superscript (g) represents the wave function and the coordinates of the ground state. These transformations give the current density of boson $\boldsymbol{j}_B(\boldsymbol{r})$ and fermion $\boldsymbol{j}_F(\boldsymbol{r})$ as

$$\boldsymbol{j}_B(\boldsymbol{r}, \tau=0) = \rho_B^{(g)}(\boldsymbol{r})\lambda_B\hat{z}, \tag{25}$$

$$\boldsymbol{j}_F(\boldsymbol{r}, \tau=0) = \rho_F^{(g)}(\boldsymbol{r})\omega_f\lambda_F\hat{z}. \tag{26}$$

If $h_{BF}=0$, the time dependences of $z_{B,F}$ become $z_B = \lambda_B \sin(\tau)$ and $z_F=\lambda_F \sin(\omega_f\tau)$; the boost parameters λ_B and λ_F correspond to the initial amplitudes of z_B and z_F, respectively.

In Fig. 2 we show the time dependence of the $z_{B,F}$ when the boson-fermion coupling $h_{BF}=-g_{BB}$ (a), $h_{BF}=-0.5g_{BB}$ (b), $h_{BF}=g_{BB}$ (c), and $h_{BF}=2g_{BB}$ (d). The dashed and solid lines represent the results of z_B and z_F, respectively. In all calculations we choose the out-of-phase at the beginning between the boson and fermion oscillations by taking the initial condition to be $\lambda_B=0.4$ and $\lambda_F=-0.4$.

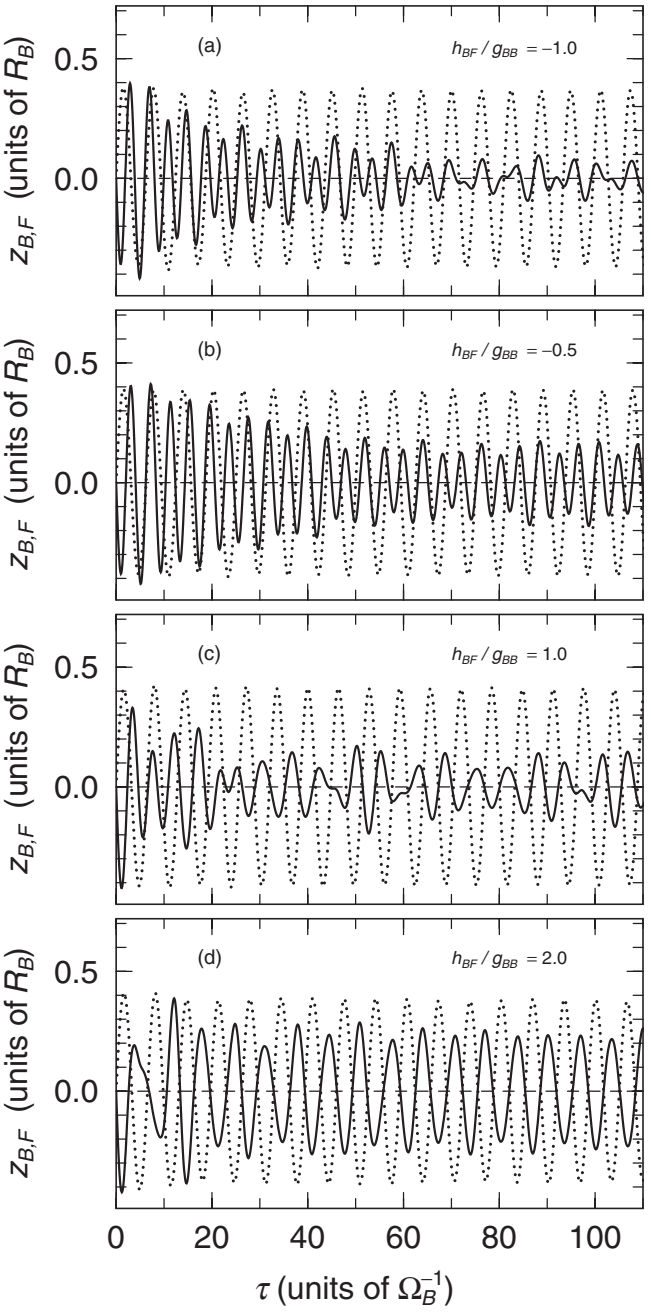

FIG. 2. Time evolution of the center-of-mass position of the boson (dotted lines) and fermion (solid lines) with the boson-fermion coupling $h_{BF}=-g_{BB}$ (a), $h_{BF}=-0.5g_{BB}$ (b), $h_{BF}=g_{BB}$ (c), and $h_{BF}=2g_{BB}$ (d). The initial condition is taken to be $\lambda_B=0.4$ and $\lambda_F=-0.4$.

While the boson oscillations are monotonous, the fermion oscillations have damping in the early time stage. When $h_{BF}=\pm g_{BB}$, the amplitude of the fermion oscillation is about 0.4 at the beginning, but it decreases and becomes about 0.1–0.2 after the damping ($\tau \gtrsim 60$). This damping becomes slower when the coupling is weaker, $h_{BF}=-0.5g_{BB}$ [Fig. 2(b)]. Furthermore, we see that after the damping z_B and z_F oscillate with the same period, and their relative phase be-

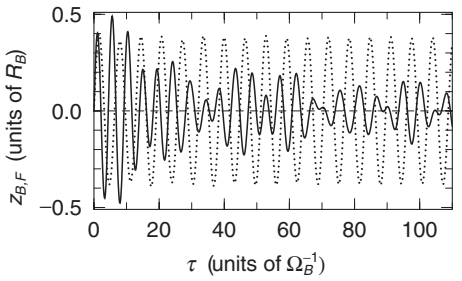

FIG. 3. Same as Fig. 2(c), but using the in-phase initial condition $\lambda_B=\lambda_F=0.4$ at the beginning.

comes in-phase when $h_{BF}<0$ and out-of-phase when $h_{BF}>0$. Note that, when $h_{BF}=2g_{BB}$, the damping of z_F is not clearly seen; the damping is too fast, and the period of the oscillation becomes the same with that of z_B in the early time stage.

In order to confirm the above comment about the relative phase after the damping, we calculate the dipole oscillation with $h_{BF}=g_{BB}$, which is started with in-phase at the beginning ($\lambda_B=\lambda_F=0.4$). The results are shown in Fig. 3. The relative phase between the boson and fermion oscillations becomes out-of-phase in the later time stage after the damping. In order to clarify it, we plot the same quantities shown in Figs. 2(a), 2(d), and 3 in later time, $120<\tau<150$, in Fig. 4. We can see that z_F oscillates almost with the same period of z_B.

As seen in Figs. 2–4, the behaviors of the fermion oscillations are not so simple and imply that the fermion oscillation includes various modes. In order to inspect these properties more, we calculate the strength function defined as the Fourier transformation of $z_{B,F}$:

$$S_{B,F}(\omega)=\int_{t_i}^{t_f} d\tau z_{B,F}(\tau)\sin(\omega\tau). \tag{27}$$

In this work we fix that $t_i=0$ and $t_f=200$ (Ω_B^{-1}). We show the strength functions of the dipole oscillations with $h_{BF}=-g_{BB}$ for the bosons (a) and the fermions (b) and with $h_{BF}=-0.5g_{BB}$ for the bosons (c) and the fermions (d) in Fig. 5, and those with $h_{BF}=g_{BB}$ for the bosons (a) and the fermions (b) and $h_{BF}=2g_{BB}$ for the bosons (c) and the fermions (d) in Fig. 6.

First we note that the boson strength functions have only one sharp peak, which is consistent with the monotonous behavior of the boson oscillations. Hence the frequency of the peak position can be considered to be the intrinsic frequency of the boson oscillation; we define ω_D^b as this frequency. Second the fermion strength has three peaks. One peak appears at $\omega=\omega_D^b$, and another peak appears at the trapped frequency, $\omega=\omega_f\approx 1.47$ in all cases, whereas the position of the other peak depends on the coupling constant. These three peaks must correspond to certain modes. For convenience we refer to these three modes as modes 1, 2, and 3 in order, and define ω_D^f as the frequency of mode 3.

The sign of the fermion strength function at $\omega=\omega_D^b$ (mode 1) is plus when $h_{BF}>0$ and minus when $h_{BF}<0$, while the signs of the strengths at $\omega=\omega_f$ (mode 2), and $\omega=\omega_D^f$ (mode 3) are minus in all oscillations. In Fig. 7, furthermore, we plot the strength functions of the bosons (a) and the fermions (b) with $h_{BF}=g_{BB}$ using the in-phase initial condition ($\lambda_B=\lambda_F=0.4$). We see that the signs of the strength functions at $\omega=\omega_f$ and $\omega=\omega_D^f$ become plus.

In this initial condition the sign of the boson strength function is always plus. The sign of the strength exhibits the relative phase between each mode and the boson oscillation; the plus and minus signs show the in-phase and out-of-phase, respectively. Then the above results imply that a choice of the phase at the beginning determines the phases of modes 2 and 3, while the phase of mode 1 is determined by the boson-fermion coupling. These results exhibit typical behaviors of the forced vibration with the external force caused by the boson oscillation, which is discussed in the following subsection.

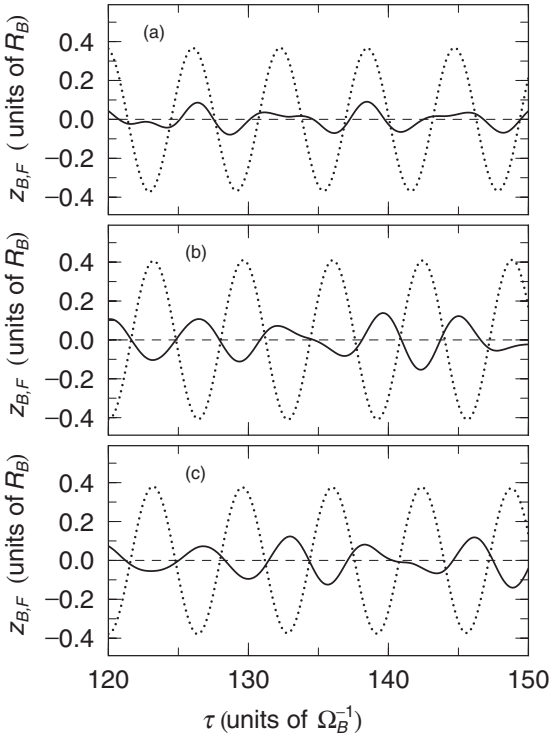

FIG. 4. Time evolution of z_B (dashed lines) and z_F (sold lines) with the boson-fermion coupling $h_{BF}=-g_{BB}$ (a), $h_{BF}=g_{BB}$ (b), and $h_{BF}=g_{BB}$ (c). In the first and second panels the oscillation is started with the out-of-phase at the beginning, and the last ones with the in-phase.

C. Modes of the fermion oscillation

In this subsection we examine the above three modes for the fermion oscillations by performing the test simulations shown in the following. First we calculate the fermion dipole oscillations with the boson motion frozen; namely, the fermions move in the fixed potential $U_F(\boldsymbol{r})$ in the ground state. In Fig. 8 we show the results with the boson-fermion coupling $h_{BF}=-g_{BB}$ (a), $h_{BF}=g_{BB}$ (b), and $h_{BF}=2g_{BB}$ (c). In each result we see a beat and damping: the amplitude of z_F oscillation is about 0.4 in the beginning, and it becomes about 0.05 after the damping.

In Fig. 9 we plot the strength functions of these fermion oscillations with the boson-fermion coupling $h_{BF}=-g_{BB}$ (a),

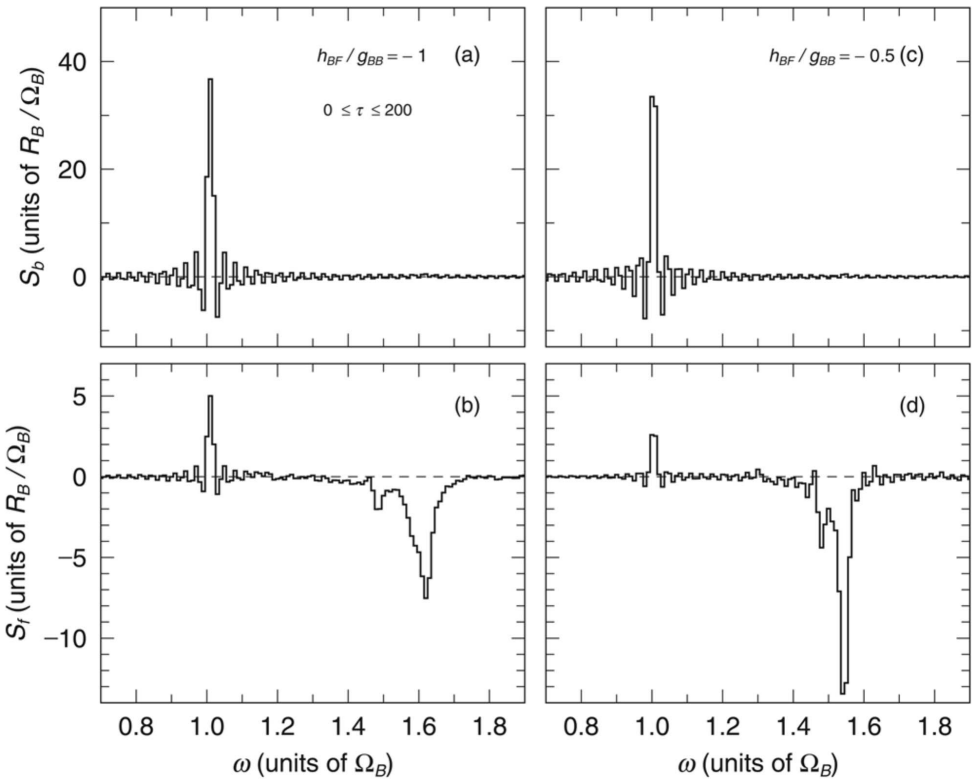

FIG. 5. Strength functions of the boson oscillation in upper panels (a),(c) and fermion oscillation in lower panels (b),(d) with $h_{BF}=-g_{BB}$ (a),(b) and with $h_{BF}=-0.5g_{BB}$ (c),(d) using the initial condition $\lambda_B=-\lambda_F=0.4$.

$h_{BF}=g_{BB}$ (b), and $h_{BF}=2g_{BB}$ (c). In all the results there are two peaks at $\omega=\omega_f$ and $\omega=\omega_D^f$, but no peak at $\omega=\omega_D^b$.

These results demonstrate that modes 2 and 3 are intrinsic modes for the fermion oscillation, and that mode 1 is caused by the boson oscillation. A mixture of modes 2 and 3 arises the beat, and this mixing and their widths make the damping in the fermion oscillations.

Next we simulate the dipole oscillation with the initial condition $\lambda_B=0.4$ and $\lambda_F=0$. In Fig. 10 we show the time dependences of z_B and z_F with the boson-fermion coupling $h_{BF}=-g_{BB}$ (a), $h_{BF}=g_{BB}$ (b), and $h_{BF}=2g_{BB}$ (c). In Fig. 11, furthermore, we plot the strength functions of the boson oscillation with $h_{BF}=-g_{BB}$ (a) and with $h_{BF}=g_{BB}$ (b) and those of the fermion oscillation with $h_{BF}=-g_{BB}$ (c) and with $h_{BF}=g_{BB}$ (d). In the fermion strength functions (c),(d) there are two peaks at $\omega=\omega_D^b$ (mode 1) and $\omega=\omega_D^f$ (mode 3), and no peak at $\omega=\omega_f$ (mode 2). In this initial condition, $\lambda_F=0$, the boson oscillation is a trigger of the fermion oscillation and moves only fermions inside of the boson occupation region. Hence these results demonstrate that mode 2 and mode 3 are the dipole motions contributed from the fermions outside and inside of the boson occupation region, respectively.

The condensed boson density distributes in a smaller region than the fermion one, so that the fermion potential U_F is separated into two regions, the inside and outside of the boson occupation region. Outside the boson occupation region the fermion potential U_F has a simple harmonic oscillator shape with the trapped frequency ω_f. Inside the boson occupation region, furthermore, the fermion potential around the central region can also be approximately described as a harmonic oscillator potential with a different trapped frequency.

Thus this fermion motion can be described with two kinds of fluids corresponding to the above two modes. One fluid moves outside the boson occupation region, and makes a dipole oscillation mode with the frequency $\omega=\omega_f$. The other fluid moving in the inside region makes the dipole oscillation with $\omega=\omega_f^D$. However the fermion potential does not have a simple harmonic oscillator shape in the boson occupation region, and then their dipole motions, particularly for the latter fluid, are not harmonic, and the oscillation amplitudes decrease.

Now we examine the above consideration in quantum calculations. We calculate the excited states in RPA and compare the results with those in our time-dependent approach. For this purpose we get the fermion wave functions in the ground states in the Hartree-Fock (HF) approximation and solve the RPA equation in the way of Ref. [28]. In the HF calculations the fermion number N_f must be dependent on the subshell closure of fermion single particle states, and changed from $N_f=1000$; for example $N_f=989$ with $h_{BF}=-g_{BB}$, but this slight change hardly affects the final results. We use seventeen particle-hole states for bosons and about five hundred ones for fermions.

Then we calculate the transition amplitudes from an excited state $|\Phi_n\rangle$ with excitation energy ω_n to the ground state $|\Phi_0\rangle$ for bosons A_B and for fermions A_F which are written as

$$A_B(\omega_n)=\langle\Phi_n|\hat{Z}_B|\Phi_0\rangle, \tag{28}$$

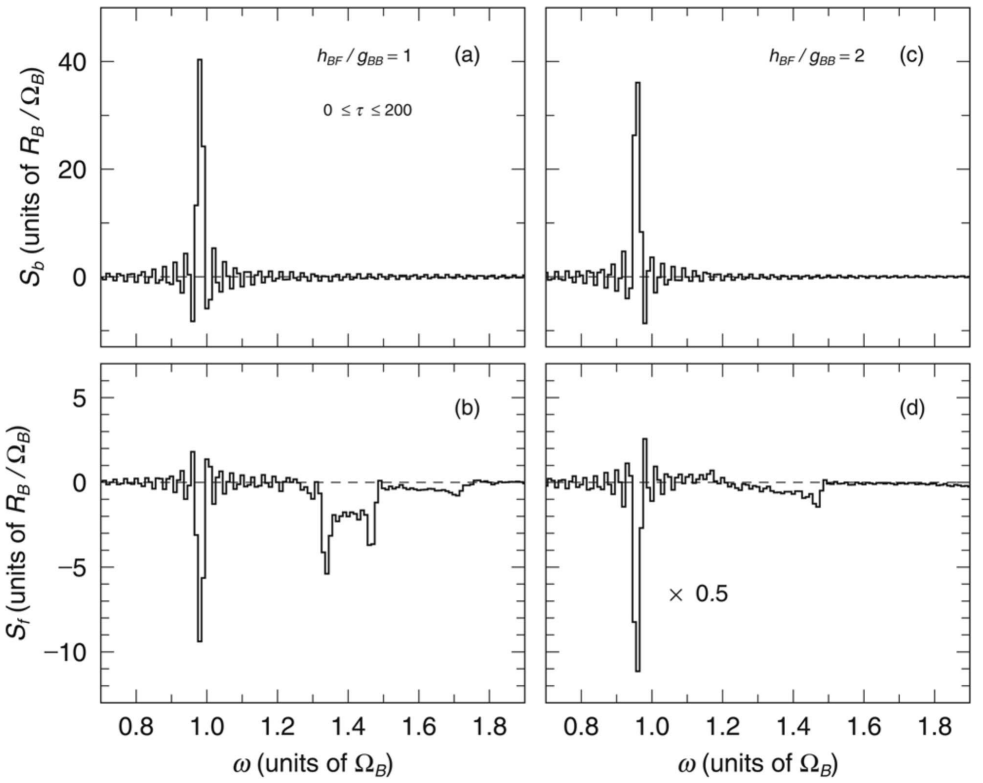

FIG. 6. Strength functions of the boson oscillation in upper panels (a),(c) and fermion oscillation in lower panels (b),(d) with $h_{BF}=g_{BB}$ (a),(b) and with $h_{BF}=2g_{BB}$ (c),(d) using the initial condition $\lambda_B=-\lambda_F=0.4$.

$$A_F(\omega_n)=\langle\Phi_n|\hat{Z}_F|\Phi_0\rangle \tag{29}$$

with

$$\hat{Z}_B=\int d^3r\phi^*(\boldsymbol{r})z\phi(\boldsymbol{r}), \tag{30}$$

$$\hat{Z}_F=\int d^3r\psi^*(\boldsymbol{r})z\psi(\boldsymbol{r}). \tag{31}$$

In Fig. 12 we show the boson $T_B(\omega_n)=3|A_B(\omega_n)|^2/4\pi$ (a) and fermion transition strengths $T_F(\omega_n)=3|A_F(\omega_n)|^2/4\pi$ (b) as functions of the excitation energy ω with $h_{BF}=-g_{BB}$.

In order to visualize the distribution for the fermion transition strength, we introduce an artificial width Γ and draw the curve of $T_F^s(\omega)$ defined as

$$T_F^s(\omega)=\frac{1}{\pi}\sum_n T_F(\omega_n)\frac{\Gamma}{\Gamma^2+(\omega-\omega_n)^2}. \tag{32}$$

In our calculation we take $\Gamma=0.01$, and plot $0.018\times T_F^s(\omega)$ in the second panel (b), where the arbitrary factor 0.018 is introduced to plot the curve with the same scale of T_F in the same figure.

In these results there is a clear peak at $\omega=1.0$ in the boson transition and two clear peaks at $\omega=1.50$ and 1.61 in the fermion transition. These two peak positions of T_F are close to the frequency of mode 2 ω_f and that of mode 3 ω_D^f in our time-dependent approach. Furthermore we see several modes with the excitation energy between ω_f and ω_D^f.

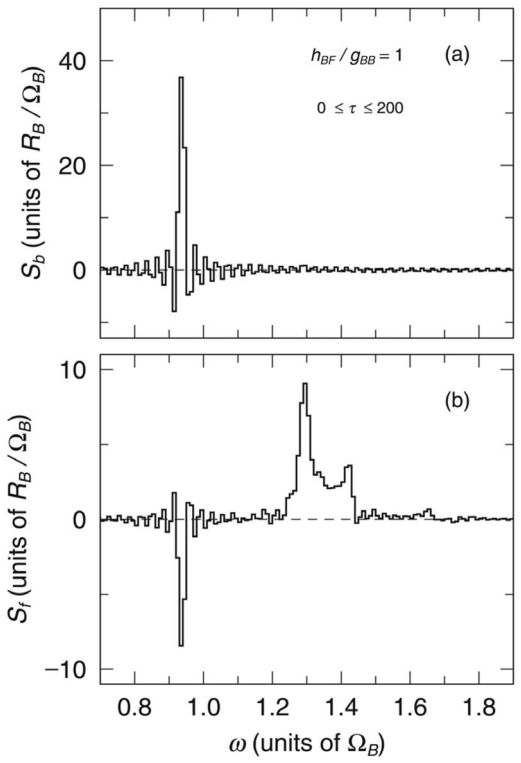

FIG. 7. The strength function of the fermion dipole oscillation with $h_{BF}=g_{BB}$, but using the in-phase initial condition $\lambda_B=\lambda_F=0.4$.

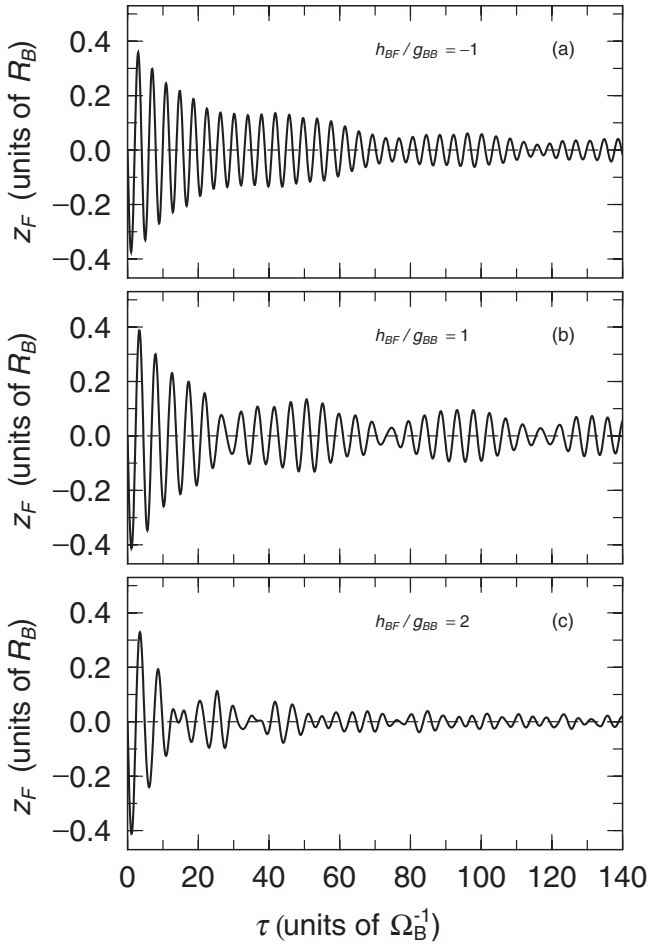

FIG. 8. Time evolution of z_F (sold lines) with the boson-fermion coupling $h_{BF}=-g_{BB}$ (a) and $h_{BF}=g_{BB}$ (b) when the boson motion is frozen.

We would like to comment that there is a peak $T_F=0.075$ at $\omega\approx 1.0$, but it is too small to be visible. In the RPA calculation, thus, there is not any strong comoving mode, and hence the fermion transitions must be almost explained as single particle processes. In Fig. 12(c) we plot the fermion transition strength, T_F, in the single particle process; the results of Figs. 12(b) and 12(c) are almost the same.

Hence the dipole oscillation behavior can be explained as follows. The condensed bosons occupy one single particle state, and the boson oscillation has one mode and does not damp. In contrast the fermions occupy many single particle states, and the fermion oscillation includes two intrinsic modes which are contributed from the Fermi gases outside and inside of the boson occupation region, respectively. Since the fermion potential cannot be critically separated, there are several modes with frequencies between ω_f and ω_D^f. Because of this statistical difference, furthermore, the boson oscillation almost one-sidedly affects the fermion oscillation. Then the fermion oscillation has one more mode caused by the external vibration force which is the boson oscillation. As a result the Fermi gas gradually loses its intrinsic modes and finally oscillates with the same frequency of the condensed Bose gas.

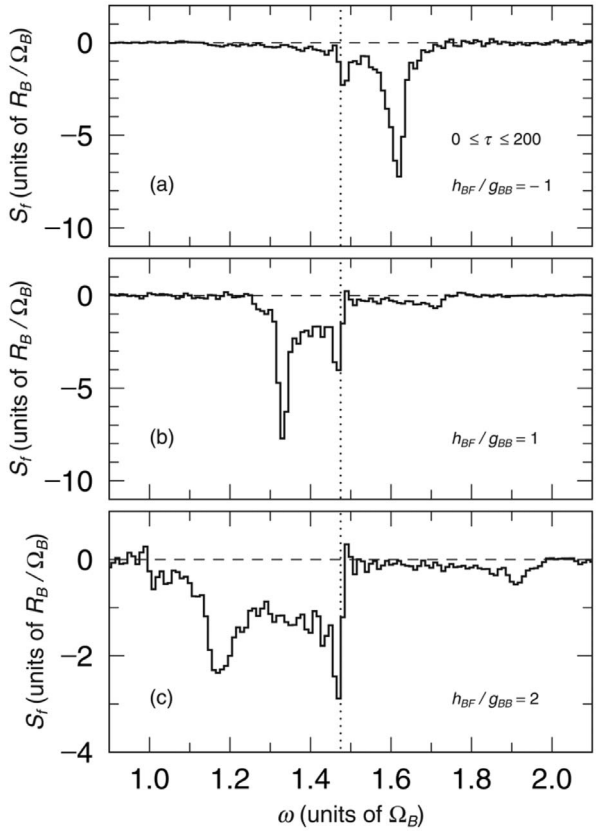

FIG. 9. Strength functions of the fermion oscillation with $h_{BF}=g_{BB}$ (a), $0.5g_{BB}$ (b), $-0.5g_{BB}$ (c), and with $h_{BF}=-g_{BB}$ (d) when the boson motion is frozen. The dotted lines indicate the fermion trapped frequency ω_f.

D. Comparison with the sum-rule approach

In this subsection we discuss the boson-fermion coupling dependence of the oscillation frequencies by comparing our results with the sum-rule approach [29]. In Fig. 13 we show the intrinsic frequencies of boson (a) and fermion (b) oscillations with full circles. For references the fermion frequencies with the boson motion frozen are plotted with the open circles which are connected with the long-dashed line, and the trapped frequency of the fermion with the dotted line in Fig. 13(b). In addition we give the results of the RPA, which is defined as the peak energy of T_F^s, with the asterisk. The three results except the sum rule are very similar and cannot be distinguished in the figure. Our results about the fermion oscillation in the full calculation (full circles) agree with those in the boson motion frozen (open circles) and those in RPA (asterisk).

The sum-rule approach [29] gives the intrinsic frequencies of the boson and fermion dipole oscillations as

$$\omega_D^b=\sqrt{1-\frac{1}{N_b}V_{DP}}, \tag{33}$$

$$\omega_D^f=\sqrt{\omega_f^2-\frac{1}{m_f N_f}V_{DP}} \tag{34}$$

with

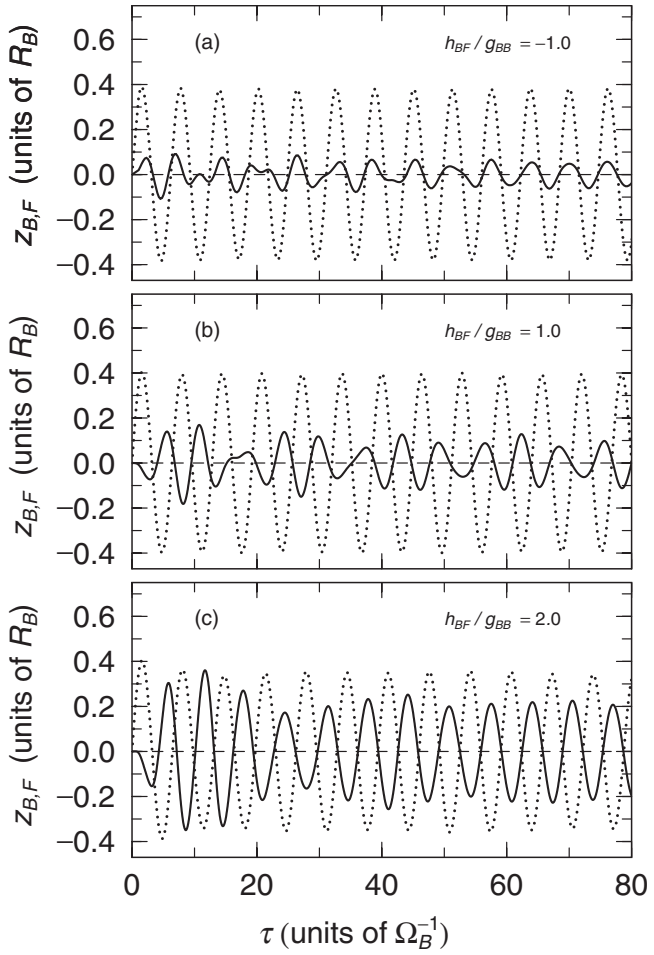

FIG. 10. Time evolution of z_B (dotted lines) and z_F (sold lines) without the boson boost at the beginning with the boson-fermion coupling $h_{BF}=-g_{BB}$ (a), $h_{BF}=g_{BB}$ (b), and $h_{BF}=2g_{BB}$ (c).

$$V_{DP}=h_{BF}\int d^3r\frac{\partial\rho_B}{\partial z}\frac{\partial\rho_F}{\partial z}. \tag{35}$$

In the same figure we also plot the results of the sum-rule approach with the thick dashed lines. The above results in the sum-rule approach agree with our results when $h_{BF}<0$, though the two results show discrepancy when $h_{BF}>0$.

It is known from Eqs. (33)–(35) that the frequency calculated with the sum-rule is sensitive to the density distribution. As discussed in Sec. III A the derivative of the fermion density with respect to the radial coordinate in the boson occupation region is negative $\partial\rho_F/\partial r<0$ when $h_{BF}\lesssim g_{BB}$ and positive $\partial\rho_F/\partial r>0$ when $h_{BF}\gtrsim g_{BB}$, while the derivative of the boson density $\partial\rho_B/\partial r<0$ in the both coupling region. As the boson-fermion coupling h_{BF} increases, hence, the fermion frequency in the sum-rule approach decreases when $h_{BF}<0$, is not varied when $0<h_{BF}<1$, and increases when $h_{BF}>0$.

The sum-rule approach is available only when the transition strength is concentrated to one excited state. In BF mixtures, however, the fermion transition strength distributes mainly to the two modes, and then the sum-rule approach cannot predict the correct intrinsic frequency of the fermion oscillations.

E. Discussions

Both our time-dependent approach and the RPA calculation explain the two modes in the fermion oscillation. However, the RPA can be available only in minimal oscillations.

Here we calculate the time evolutions z_B and z_F in RPA. By using the initial boost given in Eqs. (23) and (24) with the perturbative way, the initial state in the dipole oscillation becomes

$$|\Phi(\tau=0)\rangle=e^{i\{\lambda_B\hat{Z}_b+\lambda_F\hat{Z}_f\}}|\Phi_0\rangle\approx|\Phi_0\rangle+i\{\lambda_B\hat{Z}_b+\lambda_F\hat{Z}_f\}|\Phi_0\rangle$$
$$=|\Phi_0\rangle+i\sum_n\{\lambda_BA_B(\omega_n)+\lambda_FA_F(\omega_n)\}|\Phi_n\rangle. \tag{36}$$

This initial boost is equivalent to that given in Eqs. (23) and (24) in the first order of $\lambda_{B,F}$. Then, the time dependence of z_B and z_F are given by

$$z_B(\tau)=\frac{1}{N_b}\sum_n\langle\Phi(\tau)|\hat{Z}_b|\Phi(\tau)\rangle$$
$$=\frac{2}{N_b}\sum_nA_B(\omega_n)[\lambda_BA_B(\omega_n)+\lambda_FA_F(\omega_n)]\sin(\omega_n\tau), \tag{37}$$

$$z_F(\tau)=\frac{1}{N_f}\sum_n\langle\Phi(\tau)|\hat{Z}_f|\Phi(\tau)\rangle$$
$$=\frac{2}{N_f}\sum_nA_F(\omega_n)[\lambda_BA_B(\omega_n)+\lambda_FA_F(\omega_n)]\sin(\omega_n\tau). \tag{38}$$

In Fig. 14 we show the results for boson (dotted line) and fermions (solid line) in the out-of-phase oscillations with $h_{BF}=-g_{BB}$ (a) and $h_{BF}=g_{BB}$ (b) by using the condition $\lambda_B=-\lambda_F=\Delta z$. The amplitudes of the oscillations are scaled by Δz. Comparing these results with those in the time-dependent approach (Fig. 2), we can see a clearer beat and weaker damping in the fermion oscillations, and the period of the fermion oscillation dose not become the same as that of the boson oscillation even in the later time stage. The boson oscillation does not affect the fermion oscillation in RPA as strongly as in the time-dependent approach.

In order to inspect the reason for this difference more, we show the density distribution and the velocity fields at $\tau=0$ (a) and at $\tau=18.5$ (b) in Fig. 15. The dashed and solid contour lines represent the density distributions for boson and fermion, respectively, and the arrows indicate the fermion velocities. At both times the z component of the c.m. position of Fermi gas is zero, $z_F=0$.

At $\tau=0$ the boson and Fermi gases move with unique velocities (a) in all positions. At $\tau=18.5$, however, the velocity of the Fermi gas is directed along the contour lines of the

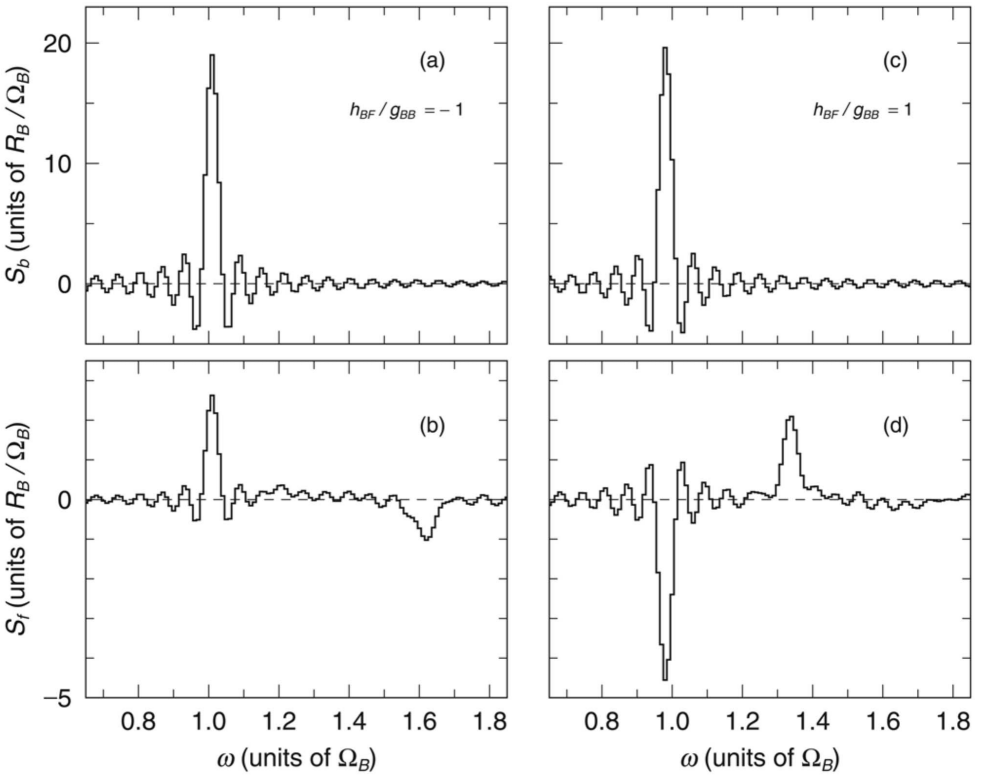

FIG. 11. Strength functions of the boson (a),(c) and fermion (c),(d) oscillations with $h_{BF}=-g_{BB}$ (a),(b) and with $h_{BF}=g_{BB}$ (c),(d). The details are shown in Fig. 10.

density, and its density becomes dilute in the space region $z<0$ and $|\mathbf{r}_T|\lesssim 1$. The Fermi gas moves to the surface part of the Bose gas because of the repulsive force from the Bose gas. This motion is very natural from the aspect of the hydrodynamics.

The RPA approach can describe only minimal oscillations with one-particle one-hole excitation energy, where the density distribution is slightly changed from that at the ground state. In the case of $h_{BF}=g_{BB}$ and the boson motion frozen, for example, its excitation energy is about 80 $\hbar\Omega_B$, and the system cannot be described with simple one-particle and one-hole states. In such non-small-amplitude oscillations the Fermi gas changes its density distribution and moves to the place with low resistance. Hence the actual oscillations of the BF mixing gases are not so simple to describe with the RPA and sum-rule approaches.

In order to confirm the above consideration, we calculate the dipole oscillations with the smaller amplitude $\lambda_B=-\lambda_F=0.05$ in our time-dependent approach. This amplitude is still larger than that in RPA, but the test particle method cannot give sufficient numerical accuracy if we use further smaller amplitude. Even in these calculations, indeed, we take the number of the test particles to be $\tilde{N}_T=400$, though it does not influence the previous results with the larger amplitude. In addition a semiclassical approach such as the Vlasov equation cannot describe discrete energy levels which appear in RPA.

In Fig. 16 we show the time dependence of z_B (dotted line) and z_F (solid line) with $h_{BF}=-g_{BB}$ (a) and $h_{BF}=g_{BB}$ (b). Comparing these results with those in Fig. 2, a beat is clearer, and damping is weaker; these results are similar to those in RPA (Fig. 14).

In Fig. 17 we show the fermion strength functions of the above dipole oscillations with $h_{BF}=-g_{BB}$ (a) and with h_{BF}

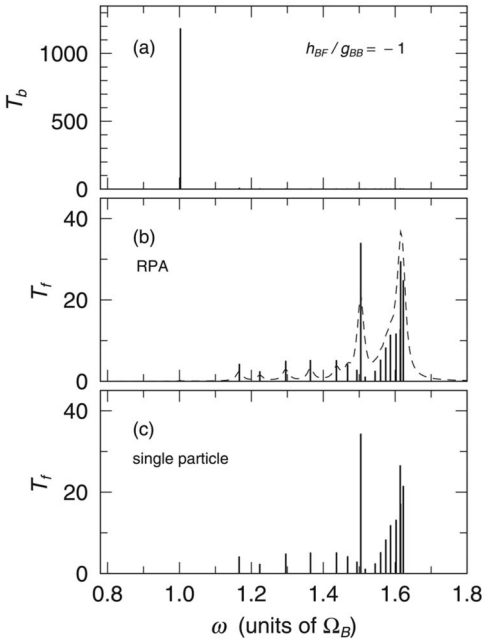

FIG. 12. Transition strengths vs the excitation energy for the boson (a) and fermion (b) oscillations with $h_{BF}=-g_{BB}$ in RPA. The fermion transition strength in the single particle process are also plotted in the bottom panel (c).

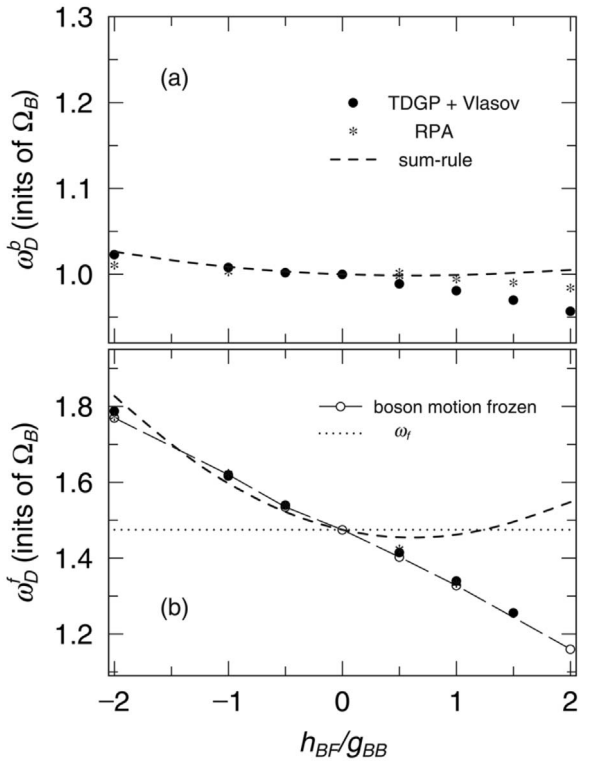

FIG. 13. Intrinsic frequencies of boson and fermion oscillations versus the boson-fermion coupling. Full diamonds and full circles represent the intrinsic frequencies of boson and fermion oscillations, respectively. The open circles, which are connected with the long-dashed line, indicate the fermion intrinsic frequency with the boson motion frozen. The thick dashed and dotted lines denote the results of the sum-rule and the trapped frequency of the fermion, respectively. The results of RPA are also plotted with asterisks, but they cannot be distinguished in the figure.

$=g_{BB}$ (c). The results are scaled by $\lambda_B=\Delta z$. Here we do not plot the boson strength functions, which do not show any different behaviors from the previous results.

For comparison we also calculate the fermion strength functions in RPA, which is obtained from Eq. (27) and Eq. (38) as

$$S_F(\omega)/\Delta z = \frac{1}{N_f}\sum A_F(\omega_n)[A_B(\omega_n) - A_F(\omega_n)]\left\{\frac{\sin[(\omega-\omega_n)t_f]}{\omega-\omega_n} - \frac{\sin[(\omega+\omega_n)t_f]}{\omega+\omega_n}\right\} \tag{39}$$

with $\lambda_B=-\lambda_F=\Delta z$ and $t_i=0$. We show the results with $h_{BF}=-g_{BB}$ in Fig. 17(c) and with $h_{BF}=g_{BB}$ in Fig. 17(d), where we use $t_f=200$ (Ω_B^{-1}). Note that the forced oscillation mode, mode-1, is caused by the term proportional to $A_B(\omega_n)A_F(\omega_n)$ in Eq. (39).

It is seen that the fermion strength calculations in the time-dependent approach are very similar to those in RPA.

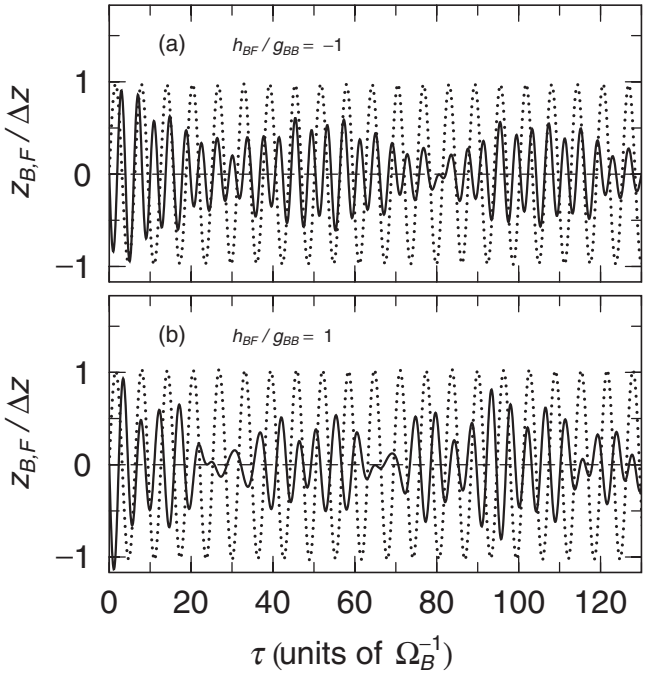

FIG. 14. Time evolutions of z_B (dashed line) and z_F (solid line) in RPA with $h_{BF}=-g_{BB}$ (a) and $h_{BF}=g_{BB}$ (b).

Particularly the peak heights at $\omega\approx\omega_D^b$ are smaller than that at $\omega\approx\omega_D^f$; namely, the contribution from the mode 1 is small. Surely results in our approach become closer to those in RPA, when the amplitude becomes smaller.

IV. SUMMARY

In this paper we study the collective dipole oscillation in the BF mixtures by solving the time evolutions of the system directly with the TDGP and Vlasov equations. The calculational results reveal that the boson and fermion oscillations make different behaviors reflected by their statistics. The condensed bosons occupy one single particle state, but the fermions distribute in many single particle states. Then the boson oscillation has only one mode and does not have damping, but the fermion collective oscillation includes vari-

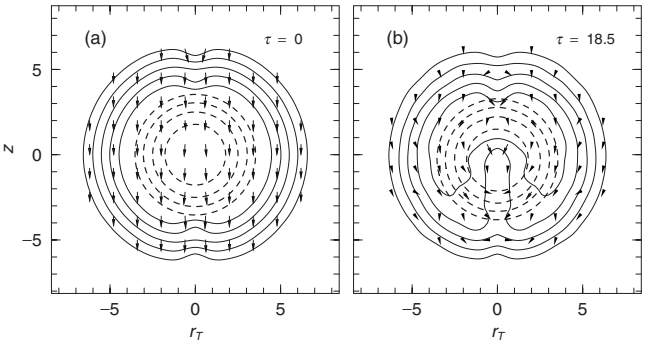

FIG. 15. Density distribution and velocity fields. at $\tau=0$ (a) and $\tau=18.5$ (b). The dashed and solid contour lines represent the density distributions of the Bose and Fermi gases, respectively, and the arrows indicate the velocities of the Fermi gas.

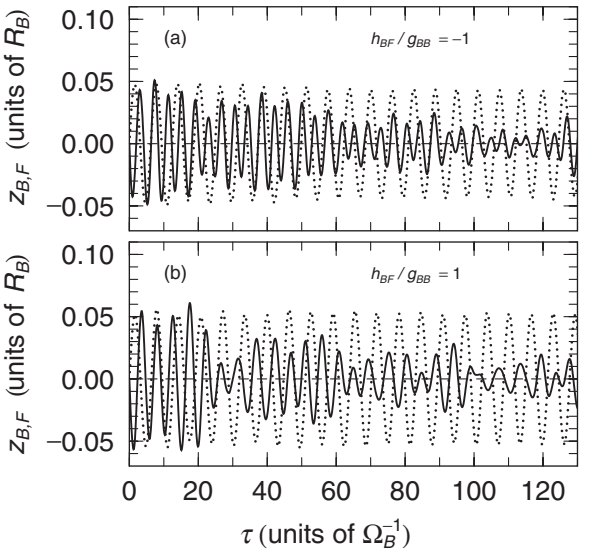

FIG. 16. Time evolutions of z_B (dashed line) and z_F (solid line) with $h_{BF}=-g_{BB}$ (a) and with $h_{BF}=g_{BB}$ (b) using the initial condition $\lambda_B=-\lambda_F=0.05$.

ous modes. In the BF mixtures, especially, the Fermi gas is separated into the two regions, inside and outside of the boson occupation region, and these two fluids oscillate with different periods.

Furthermore the boson oscillation almost one-sidedly affects the fermion oscillation, and then the fermion oscillation includes three modes: one is a mode of the forced vibration caused by the boson oscillation, the other modes are two fermion intrinsic modes contributed from the Fermi gases inside and outside of the boson occupation region, respectively. In addition there are several small modes in the fermion oscillations with frequencies between the two intrinsic frequencies. These modes cause the beat and damping in the fermion oscillation. As the result the fermion motion gradually loses the strength of its intrinsic modes and finally oscillates with the same frequency of the condensed Bose gas.

The RPA approach can also explain the frequencies of the boson and fermion intrinsic modes. The qualitative behavior of the strength function in RPA oscillations is similar to that in our approach. Nevertheless the time evolutions of z_F are not the same, particularly in the later time stage, because the forced oscillation modes, mode 1, does not largely contribute to the whole oscillation in RPA. RPA is available only in the minimal oscillation, and cannot describe the change of the density distribution in the time evolution process. In actual experiments the amplitude is not so small, and hence we must solve the time-dependent process of the collective oscillations directly.

In this work we do not take into account two-body collisions and thermal bosons [42]. In the system $N_b \gg N_f$ at zero temperature, the thermal bosons are very few, and then the two body collisions do not play significant roles in the dynamical process. However, it is not easy to establish gases at such low temperatures in actual experiments. In the future we need to introduce the two body collision terms into our approach [43,44].

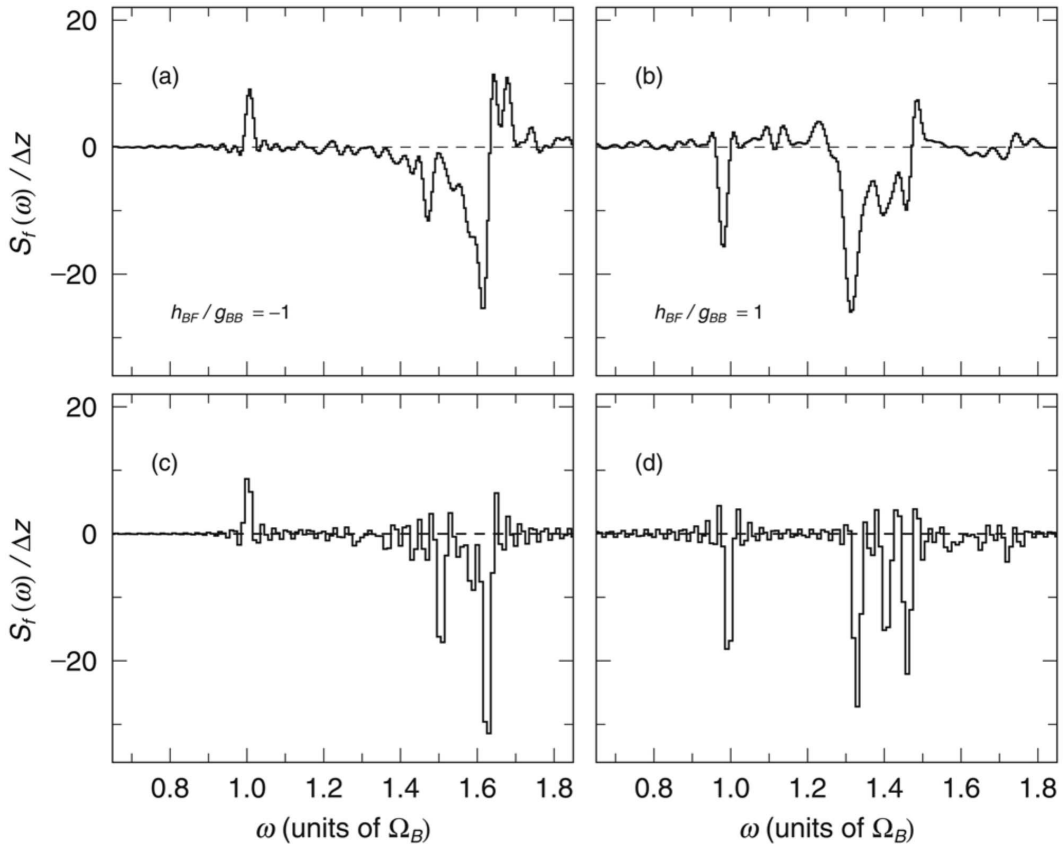

FIG. 17. Strength functions of the fermion oscillations with $h_{BF}=-g_{BB}$ (a),(b) and with $h_{BF}=g_{BB}$ (c),(d) using the initial condition $\lambda_B(=\Delta z)=-\lambda_F=0.05$. The results in the time-depent approach are shown in upper panels (a),(c) and those in RPA are shown in lower panels (b),(d).

[1] E. A. Cornell and C. E. Wieman, Rev. Mod. Phys. **74**, 875 (2002); W. Ketterle, *ibid.* **74**, 1131 (2002).
[2] F. Dalfovo *et al.*, Rev. Mod. Phys. **71**, 463 (1999).
[3] C. J. Pethik and H. Smith, *Bose-Einstein Condensation in Dilute Gases* (Cambridge University Press, Cambridge, 2002).
[4] J. O. Andersen, Rev. Mod. Phys. **76**, 599 (2004).
[5] A. G. Truscott, K. E. Streker, W. I. McAlexander, G. B. Partridge, and R. G. Hulet, Science **291**, 2570 (2001); G. Roati, F. Riboli, G. Modugno, and M. Inguscio, Phys. Rev. Lett. **89**, 150403 (2002).
[6] B. DeMarco and D. S. Jin, Science **285**, 1703 (1999); S. R. Granade, M. E. Gehm, K. M. OHara, and J. E. Thomas, Phys. Rev. Lett. **88**, 120405 (2002).
[7] F. Schreck, L. Khaykovich, K. L. Corwin, G. Ferrari, T. Bourdel, J. Cubizolles, and C. Salomon, Phys. Rev. Lett. **87**, 080403 (2001).
[8] A. G. Truscott, K. E. Strecker, W. I. McAlexander, G. B. Partridge, and R. G. Hullet, Science **291**, 2570 (2001); Z. Hadzibabic, C. A. Stan, K. Dieckmann, S. Gupta, M. W. Zwierlein, A. Görlitz, and W. Ketterle, Phys. Rev. Lett. **88**, 160401 (2002); Z. Hadzibabic, S. Gupta, C. A. Stan, C. H. Schunck, M. W. Zwierlein, K. Dieckmann, and W. Ketterle, *ibid.* **91**, 160401 (2003).
[9] M. Modugno, F. Ferlaino, F. Riboli, G. Roati, G. Modugno, and M. Inguscio, Science **297**, 2240 (2002); Phys. Rev. A **68**, 043626 (2003).
[10] H. Feshbach, Ann. Phys. (N.Y.) **19**, 287 (1962).
[11] K. Mølmer, Phys. Rev. Lett. **80**, 1804 (1998).
[12] M. Amoruso, A. Minguzzi, S. Stringari, M. P. Tosi, and L. Vichi, Eur. Phys. J. D **4**, 261 (1998).
[13] T. Miyakawa, K. Oda, T. Suzuki, and H. Yabu, J. Phys. Soc. Jpn. **69**, 2779 (2000).
[14] M. J. Bijlsma, B. A. Heringa, and H. T. C. Stoof, Phys. Rev. A **61**, 053601 (2000).
[15] L. Vichi, M. Inguscio, S. Stringari, and G. M. Tino, Eur. Phys. J. D **11**, 335 (2000).
[16] L. Vichi, M. Inguscio, S. Stringari, and G. M. Tino, J. Phys. B **31**, L899 (1998).
[17] N. Nygaard and K. Mølmer, Phys. Rev. A **59**, 2974 (1999).
[18] X. X. Yi and C. P. Sun, Phys. Rev. A **64**, 043608 (2001).
[19] L. Viverit, C. J. Pethick, and H. Smith, Phys. Rev. A **61**, 053605 (2000).
[20] P. Capuzzi and E. S. Hernández, Phys. Rev. A **66**, 035602 (2002).
[21] P. Capuzzi, A. Minguzzi, and M. P. Tosi, Phys. Rev. A **68**, 033605 (2003).
[22] T. Miyakawa, T. Suzuki, and H. Yabu, Phys. Rev. A **64**, 033611 (2001).
[23] R. Roth and H. Feldmeier, Phys. Rev. A **65**, 021603(R) (2002).
[24] T. Miyakawa, T. Suzuki, and H. Yabu, Phys. Rev. A **62**, 063613 (2000).
[25] A. Minguzzi and M. P. Tosi, Phys. Lett. A **268**, 142 (2000).
[26] P. Capuzzi and E. S. Hernández, Phys. Rev. A **64**, 043607 (2001).
[27] S. K. Yip, Phys. Rev. A **64**, 023609 (2001).
[28] T. Sogo, T. Miyakawa, T. Suzuki, and H. Yabu, Phys. Rev. A **66**, 013618 (2002); T. Sogo, T. Suzuki, and H. Yabu, *ibid.* **68**, 063607 (2003).
[29] T. Miyakawa, K. Oda, T. Suzuki, and H. Yabu, J. Phys. Soc. Jpn. **69**, 2779 (2000).
[30] X. J. Liu and H. Hu, Phys. Rev. A **67**, 023613 (2003).
[31] T. Maruyama, H. Yabu, and T. Suzuki, Phys. Rev. A **72**, 013609 (2005).
[32] G. F. Bertsch, Nucl. Phys. **249**, 253 (1975); D.M. Brink and R. Leobardi, Nucl. Phys. **A258**, 285 (1976).
[33] G. F. Bertsch and K. Stricker, Phys. Rev. C **13**, 1312 (1976); T. Suzuki, Prog. Theor. Phys. **64**, 1627 (1980).
[34] D. S. Jin, J. R. Ensher, M. R. Matthews, C. E. Wieman, and E. A. Cornell, Phys. Rev. Lett. **77**, 420 (1996); M.-O. Mewes, M. R. Andrews, N. J. van Druten, D. M. Kurn, D. S. Durfee, C. G. Townsend, and W. Ketterle, *ibid.* **77**, 988 (1996).
[35] T. Kimura, H. Saito, and M. Ueda, J. Phys. Soc. Jpn. **68**, 1477 (1999); R. Graham and D. Walls, Phys. Rev. A **57**, 484 (1998); D. Gordon and C. M. Savage, Phys. Rev. A **58**, 1440 (1998).
[36] F. Chevy, V. Bretin, P. Rosenbusch, K. W. Madison, and J. Dalibard, Phys. Rev. Lett. **88**, 250402 (2002).
[37] M. Tohyama, Phys. Rev. A **71**, 043613 (2005).
[38] S. Potting, M. Cramer, W. Zhang, and P. Meystre, Phys. Rev. A **65**, 063620 (2002); C. P. Search, H. Pu, W. Zhang, and P. Meystre, Phys. Rev. Lett. **88**, 110401 (2002).
[39] L. P. Kadanoff and G. Baym, *Quantum Statistical Mechanics* (Benjamin, New York, 1962).
[40] R. W. Hockney and J. W. Eastwood, *Computer Simulations Using Particles* (McGraw-Hill, New York, 1981); C. Y. Wong, Phys. Rev. C **25**, 1460 (1982).
[41] E. G. M. van Kempen, S. J. J. M. F. Kokkelmans, D. J. Heinzen, and B. J. Verhaar, Phys. Rev. Lett. **88**, 093201 (2002).
[42] B. Jackson and E. Zaremba, Phys. Rev. A **66**, 033606 (2002).
[43] G. F. Bertsch and S. Das Gupta, Phys. Rep. **160**, 189 (1988).
[44] T. Maruyama, W. Cassing, U. Mosel, and K. Weber, Nucl. Phys. A **573**, 653 (1994).